Optimization of Adsorption Parameters Using Central Composite Design for the Removal of Organosulfur in Diesel Fuel by Bentonite-Supported Nanoscale NiO-WO_3

Pedram, Toktam; Es'haghi, Zarrin
Department of Chemistry, Payame Noor University (PNU), Tehran, I.R. IRAN

Ahmadpour, Ali
Department of Chemical Engineering, Faculty of Engineering, Ferdowsi University of Mashhad, I.R. IRAN

Nakhaei, Ahmad*[+]
Young Researchers and Elite Club, Mashhad Branch, Islamic Azad University, Mashhad, I.R. IRAN

ABSTRACT: *Desulfurization using porous materials is based on the capability of a solid sorbent to selectively adsorb organic sulfur-containing compounds. In the present study, different sorbents were prepared by varying the NiO/WO_3 loadings onto bentonite for the removal of sulfur from commercial diesel fuel containing approximately 100 ppm total sulfur (S). X-Ray Diffraction (XRD), Fourier Transform InfraRed (FT-IR) spectroscopy, and Scanning Electron Microscopy (SEM) showed the ability of modified bentonite to adsorb dibenzothiophene (DBT) depends strongly on the surface chemistry, particularly on the presence of basic oxygen-containing groups and acid content. A Plackett–Burman Design (PBD) was chosen as a screening method to estimate the relative influence of the factors that could have an influence on the analytical response. The significant variables included: sorbent amount, feed volume, extraction solvent kind, and its volume were optimized using Central Composite Design (CCD). 93.5% removal of sulfur was observed with $NiO@WO_3$@bentonite.*

KEYWORDS: *Nanoparticles; Metallic composites; Desulfurization; Diesel fuel.*

INTRODUCTION

Novel environmental regulations regarding the sulfur content in oil fuel products have forced researchers and refineries to extend efficient processes for producing cleaner fuels [1-3]. Mainly, oil products with an ultra-low sulfur content (<1 ppm) are required in several cases like the fuel cells application. Therefore, ultra-deep desulfurization of liquid hydrocarbon fuels has become an increasingly essential subject worldwide. Besides, the traditional hydrodesulphurization (HDS) by CoMoS or NiMoS-based catalysts are the established processes

* *To whom correspondence should be addressed.*
+ E-mail: *nakhaei_a@yahoo.com ; nakhaei_a@mshdiau.ac.ir*
1021-9986/2022/3/808-820 13/$/6.03

in petroleum refineries for the production of desulfurized transportation fuels similar to gasoline, diesel, and jet fuels. In spite of the best high efficiency and the technological importance of HDS, dibenzothiophenes and particularly 4, 6-dimethyldibenzothiophene which is considered resistant to chemical reactions, cannot be totally removed by this process. Thus, research efforts have focused recently on the novel, alternative methods. Such as adsorptive desulfurization and oxidative desulfurization have been explored [4-6].

Among all these alternative desulfurization techniques, ADS has attracted the extensive attention of several research groups to produce ultra-clean fuels due to the saving of energy and operation costs. Many researchers used ADS method for the removal of sulfur compounds from diesel, gasoline, jet, or model fuels using porous materials, such as charcoal [7] mesoporous silica [8], metal cation-exchanger microporous zeolites [9, 10], and transition metal compounds supported on porous silica gel [11]. In this paper, bentonite was used as the base adsorbent. It is beneficial for the treatment of environmental pollution because of its large surface area, excellent swelling capacity, high adsorption capacity, and low-cost [12-14]. Bentonite has been used as a binder of oxide material like; iron, zinc, chromium, Cu, cobalt, and titanium oxides [15] for SO_2, [16-18] dibenzothiophene, [19] and Chattonella marina [20]. However, raw bentonites usually exhibit a small surface area due to the strong restack of layers, limiting their application in dye removal. Modification such as acid activation and thermal treatment has been performed to expand the surface area and enlarge the pore size of bentonites. However, such modification may result in the destruction of bentonites and reduce the sum of the reactive surface sites, thus having a detrimental effect on the uptake capacity.

In the past decades, modification with metals and oxides for example Al, Fe, Ti, Ni, Cu, and Ag [21-23] has been used to improve and increase the properties of bentonites. Ni-based sorbents exhibited improved performance for ultra-deep desulfurization of liquid hydrocarbons due to high sulfur capacity and selectivity [24]. Reported that Ni-based sorbents were very efficient in selective removal of T, BT, and DBT from commercial and model fuels. Ni has a unique sponge texture and bears the merits of high surface area (ca. 100 m^2/g), high porosity (ca. 0.1 cm^3/g), large pore size (ca.4 nm), low cost, and ready availability [12, 13], thus having the potentiality to be a practical desulfurization adsorbent or clean fuel production. Also, among these materials, nano-sized tungsten trioxide materials have attracted much attention for the removal of organic dyes because of their environmentally benign nature and excellent adsorption properties. To date, various structures based on WO_3, such as nanorods, nanoplates, and nanodiscs have been successfully fabricated and applied in adsorption processes [12, 13]. In the present paper, the major objective is to study the efficiency of modified bentonite with Ni and W for DBT removal. The effect of impregnating metal ions onto the bentonite on its adsorption performance was explored. The modified NiO/WO_3 composites show excellent DBT detecting and highly efficient adsorption properties. With physical and chemical properties (i.e., large specific surface area and adsorptive affinity for organic and inorganic ions), bentonite is increasingly attracting widespread attention as a new kind of microporous solid that can serve as separating agents or sorbents, etc. The adsorption characteristics of DBT on sorbents were studied by using a dynamic adsorption method. The chemical, morphological, and thermal degradation properties and surface area were characterized by using FT-IR, SEM, and XRD analysis methods. The experimental conditions were optimized based on the results obtained from the Plackett–Burman Design (PBD) using a Central Composite Design (CCD).

EXPERIMENTAL SECTION

Materials

In this study, raw bentonite was obtained from Zarinkhak Ghayen, Iran. DBT was purchased from Aldrich (USA). N-heptane, Na_2WO_4, Ni $(NO_{3)2}$. $9H_2O$, HNO_3, H_2SO_4 methanol, and ethanol were purchased from Merck Company (Darmstadt, Germany).

All chemicals were of analytical grade and used without further purification. Deionized double distilled water was used throughout all the experiments.

The stock solution of 100 mg/L DBT was prepared and saved at 4 ^oC. Working standard solutions were obtained by sufficient dilution of the stock standard solutions.

Instrumentation

The Fourier Transform InfraRed (FT-IR) spectroscopy, Thermo Nicolet Avatar- model 560 (USA) operating

in transmission mode was used to characterize the surface of magnetic nanoparticles. The nanoparticles were ground with KBr and compressed into a pellet whose spectra were recorded. The morphology of the clays used in the adsorption study was examined by the field emission scanning electron microscope (FE-SEM) TESCAN model MIRA3-FIG (Česko). The adsorbents were characterized by determining their surface area, pore diameter, and pore volume, SEM in order to know about their nature of the adsorbents. The mineralogical composition of the clays used in the adsorption study was examined by the mentioned SEM too. The crystalline structure of the adsorbents was confirmed by powder X-ray diffraction by using a Siemens D−500 X-ray diffractometer (Germany), equipped with Ni−filtrated Cu K α radiation (40 kV tube voltage, 100 mA tube current, and λ =0.154nm). Experimental design and analysis of the experiments were done using Minitab Release 16 Statistical Software.

Adsorbent Preparation.

Preparation of bentonite as adsorbent

10 g of raw bentonite was obtained from Zarinkhak Ghayen taken in a round bottom flask and 200 mL of 0.1 M HNO_3 and 0.1 M H_2SO_4 solutions were added to it. The bentonite and acid solutions in the flask were refluxed with continuous stirring and heating (90 °C) for 3 h. After 3 h the bentonite slurry was filtered by a Buchner funnel, then washed with distilled water, dried at 110°C in the oven, and stored for further use**.**

Preparation of nano bentonite

In summary, a suspension of 0.8 g of the pretreated bentonite in 50 mL ethanol was prepared and sonicated with Powers 50-W. The suspension was ultrasonically irradiated for 4h, at (25 °C). The nanostructures bentonite was calcined at (800 °C) for 4h [25].

Preparation of nanocomposites

The first 10 g nano bentonite and 4.28g Ni $(NO_3)_2.9H_2O$, 4.28 g Na_2WO_4 were added to the flask with 200 mL distilled water, then these solutions were refluxed with continuous stirring and heating (60 °C) for 24 h. Solution slurry was filtered and then dried at (110 °C) in the oven for 24h. Nanostructures bentonite was calcined at (400 °C) for 4h.

Sulfur adsorption experiments

Batch adsorption experiments were performed at (60 °C) temperature for 20 min in order to remove sulfur from a model fuel made from n-heptane mixed with a known-trace amount of dibenzothiophene. In each test, 0.01 g of the prepared adsorbent was added to 12 mL of the model fuel (0.01 g sorbent / 12mL model fuel) and the mix was shaken for 20 min. The experiments were carried out under optimal conditions. The concentration of DBT in model oil was determined by UV-Visible Spectrophotometer (Schimadzu, 2010, Japan) at a wavelength of 325 nm. The adsorbed amount of sulfur was calculated directly from breakthrough curves.

$$\text{Desulfurization ratio (\%)} = [(C_0 - C)/C_0] \times 100$$

Where C_0 is the initial molar concentration of sulfur (mol/L), and C is the final molar concentration of sulfur (mol/L).

Adsorption isotherm studies

Research on the variation of initial DBT solutions with concentrations ranging from 5 mg/L to 180 mg/L was used. In stopper Erlenmeyer flasks, 0.01 g of the adsorbents and 12mL of the solutions were added and stirred at 3000 rpm for 20 min maintained at (60 °C). The Langmuir and Freundlich isotherm models were used to explain the adsorption equilibrium. From these models, the adsorption performance of the adsorbents could be evaluated. The adsorption capacity of the adsorbent was calculated, and equation constants that give indications of adsorption performance were also determined. The amount of DBT adsorbed is calculated by:

$$q = \frac{(C_e - C_0)\,V}{W} \quad (1)$$

Where q (mg/g) is (the amount of adsorbate adsorbed in mg)/(amount of adsorbent used for adsorption expressed in gram). C_0 and C_e are the initial and equilibrium concentrations of DBT (mg/L) in the solution, V is the volume of solution (L), and W is the weight of adsorbent (g) in the mixture. Adsorbed amounts per unit weight for DBT removal at 50, 60, 80.100,150 and 180 mg/L initial concentrations and 20 min time are: 59.64, 71.58, 95.45, 119.28, 178.59, 243.10 mg/g, respectively. The isotherm data are tested with Freundlich and Langmuir models for further investigation.

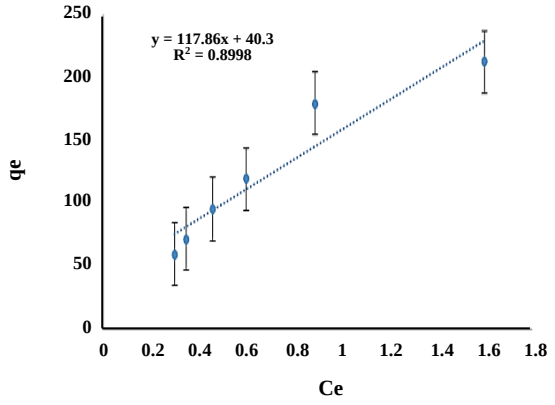

Fig. 1: Adsorption isotherm of DBT on modified bentonite.

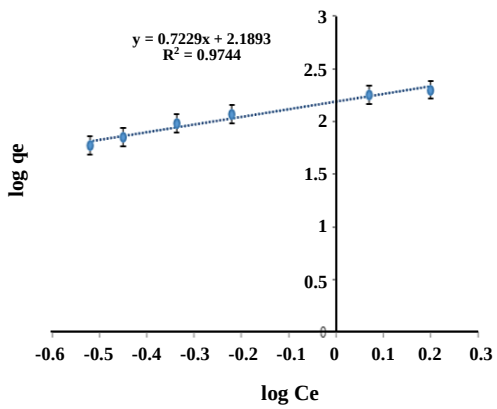

Fig. 2: Freundlich plot of DBT at 60 °C.

Adsorption Isotherms

The relationship of the amount of DBT adsorbed, *qe* (mg/g) per gram of NiO@WO_3@bentonite was studied. Nanocomposite with the equilibrium concentrations C_e (mg/L) is shown in Fig. 1. A study on the variation of initial DBT concentration at a fixed amount of adsorbent (0.01 g) per 12 mL solution was carried out at a temperature (60 °C). The adsorption isotherms for DBT sorption on adsorbent were obtained for concentrations ranging from 5 to 180 mg/L, while keeping all other parameters constant. These parameters were: shaking time = 20 min, stirring speed = 3000 rpm. *qe* increased sharply with an increase of C_e and then adsorption of the monomolecular layer reached saturation i.e. q_e is close to the maximum adsorption amount (q_m).

Freundlich model

Langmuir and Freundlich's equations are usually used for describing the adsorption equilibrium used for DBT treatment applications. Freundlich's model very gives a better fit, particularly for adsorption from liquids, and can be expressed as [26]:

$$q_e = \frac{K_f C_1}{n} \quad (2)$$

Where K_f and n are Freundlich constants related to adsorption capacity and adsorption intensity. The plot for the adsorption of DBT on adsorbent is shown in Fig. 2. It is seen that the model gives an excellent fit to the experimental data with the correlation coefficient of $R^2 = 0.9744$. Usually, for a good adsorbent n is in this range: $1 < n < 10$. A smaller value of n indicates better adsorption and the formation of a relatively powerful bond between adsorbate and adsorbent.

Langmuir model

Langmuir adsorption isotherm is given by the following equation

$$\frac{C_e}{q_e} = \frac{1}{q_m b} + \frac{1}{q_m} c_e \quad (3)$$

In the model, q_m (mg/g) is the amount of adsorption corresponding to complete monolayer coverage and b (L/mg) is the Langmuir constant related to the energy or net enthalpy of adsorption [27]. When C_e/q_e is plotted against C_e, a straight line with the slope of $1/bq_m$ is obtained in Fig. 3. The plot indicates that the adsorption of DBT follows the Langmuir isotherm. A host of research workers have applied this model to interpret their sorption data [28, 29]. In the present paper, we have observed that the Langmuir plot gives a fairly well fit to the experimental data with $R^2 = 0.9529$. The values of Freundlich and Langmuir's constants obtained from the plots are given in Table 1 for comparison. It is seen that the Langmuir model fitted the results a little better than the Freundlich model. It should be mentioned that the separation factor (*RL*) value indicates the type of isotherm. RL values between 0 and 1 suggest favorable adsorption [30].

$$R_L = 1/\left(1 + C_0 \times b\right) \quad (4)$$

Where b is the Langmuir constant and C_0 is the initial adsorbate concentration (mg/L). *RL* values of DBT presented in Table 2 are between 0 and 1 for all concentrations at 60 °C, indicating favorable adsorption.

Table 1: Fitted isotherm models for the adsorption of DBT on modified bentonite.

Model	Linearized equation	Parameters	R2
Freundlich	Ln(qe) = Ln(Kf) + 1nLn(Ce)	Kf = 0.78 n =1.96	0.9744
Langmuir	Ce/qe= 1/qmb+ 1 /qm .Ce	qm =243.9 b =1.96	0.9529

Table 2L RL values for adsorption of DBT onto modified bentonite at 60 °C.

DBT initial concentration, mgL^{-1}	50	60	70	80	100	150	180
R_L	0.001	0.0084	0.007	0.0063	0.005	0.0034	0.0028

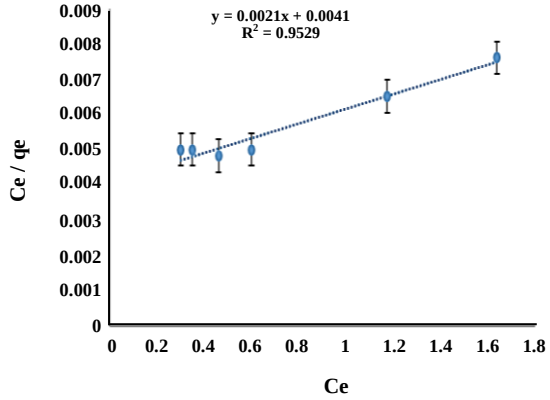

Fig. 3: Langmuir plot of DBT at 60 °C.

Thermodynamic parameters

The temperature effect on the adsorption of DBT on NiO@WO_3@bentonite nanocomposite was explained more by thermodynamic parameters. Thermodynamic parameters i.e. change in free energy (ΔG^o); change in enthalpy (ΔH^o) and change in entropy (ΔS^o) were investigated by the next equations [31]:

$$\Delta G^{o} = -RT \ln K_D \quad (5)$$

$$\ln K_D = \frac{\Delta S^{o}}{R} - \frac{\Delta H^{o}}{RT} \quad (6)$$

$$\ln K_D = \frac{qe}{Ce} \quad (7)$$

Where K_D is the distribution coefficient, R is the ideal gas constant (8.314 J/mol.K) and T is the absolute temperature in Kelvin. Ln K_D was plotted versus 1/T as given in Fig. 4. The value of ΔH^o and ΔS^o was calculated from the slopes and intercepts of the linear plot in K_D versus 1/T while the value of ΔG^o was calculated through Eq. (5). The value of ΔG, ΔH^o , and ΔS^o is given in Table 3. The value of ΔG^o is negative which indicates that the adsorption was spontaneous. The value of ΔS^o is positive which suggests that the DBT molecule was adsorbed randomLy on the surface of the adsorbent; while the positive value of ΔH^o confirms that the adsorption process was endothermic.

RESULTS AND DISCUSSION

Sorbents characterization

The elemental analysis (mass %) showed the composition of the bentonite to be: SiO_2, ~67.8; Al_2O_3, ~11.5; Fe_2O_3, ~2.1; MgO, ~2.34; CaO, ~1.4; CaO, ~1.4; Na_2O, ~0.31; and K_2O, ~0.14. DBT has been used as a model, compound to measure the extent of activity of the sorbents toward sulfur compounds' adsorption. To obtain the model oil for desulfurization, DBT was placed into n-heptanes, and in the final solution, the sulfur concentration was 100 ppm.

FTIR Spectra of the Sorbents

"Figs. 5a–b." shows the FT-IR spectrum of natural Na-bentonite and modified sample. A sharp intense band at 3629.5cm^{-1} assigned to OH stretching vibrations of bentonite and attributed to the inner hydroxyl units within the clay layers, in the 4000–3000 cm^{-1} range. The band at 3629 cm^{-1} is responsible for free un-complexed hydroxyls, as well as the band 1643 cm^{-1} is responsible for bending H–O–H vibration in the water. The band 3425 cm^{-1} is responsible for hydroxyls bound via hydrogen bonds. The very strong absorption band at 1037.6 cm^{-1} is due to Si–O bending vibration [32]. The band 1384 cm^{-1} is attributed to C–H scissoring vibrations of CH_3-N^+ moiety [33]. The peak observed at 794.6 cm^{-1} is assigned to the stretching vibration of Si- O [34]. Peaks at 520.9 cm^{-1} and 470 cm^{-1}

Table 3: Thermodynamic parameters for the adsorption of DBT onto modified bentonite.

ΔH° (kJ/mol)	ΔS° (kJ/mol K)	ΔG° (kJ/mol)				
-56.83	0.23	288K	298K	308K	318K	322K
		-7.854	-13.007	-15.185	-16.418	-18.23

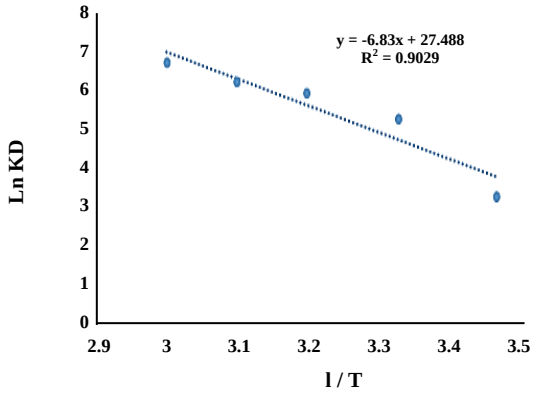

Fig. 4: Van't Hoff plots for the adsorption of DBT onto modified bentonite.

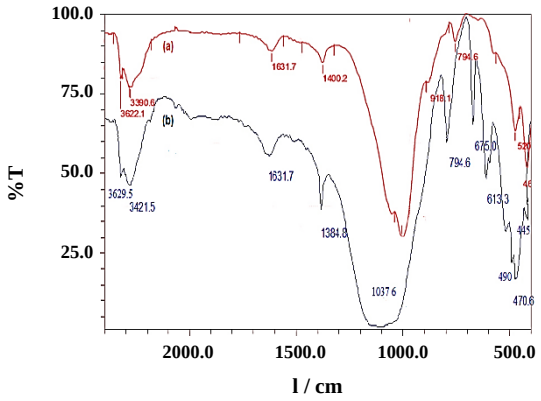

Fig. 5: FT-IR spectra of adsorbents at 60 °C: raw bentonite (a) and NiO@WO3@bentonite (b).

are referred to Si-O-Al and Al-OH respectively [35-37]. Two new peaks were shown at 445 and 490 cm-^{1} in spectrum Fig. 5b. These peaks were assigned to Ni–O stretching as was reported in the literature [38].

Surface morphological study of the prepared adsorbents

The morphological study of the prepared adsorbents was carried out with scanning electron microscopy (SEM) in order to check its surface and porosity. Pores present in the adsorbent surface have a high role in the adsorbate adsorption. Usually, the adsorbent with porous and rough morphology has a high adsorption capacity [39-41]. The morphologies of the Na-Bentonite and NiO@WO_3@bentonite are shown in Figs. 6a and 6b respectively. The bentonite consisted of large area nanosheets that can be seen clearly in Fig. 6b. As well, the layered structure with larger pores can be seen. The surface is mainly comprised of irregularities and plateaus. The textural non-uniformity is evident in both magnifications. The particle size, though, seems of uniform size as compared to the original clay. It shows that Ni and W cations are uniformly dispersed on the entire surface of the clay, and it can be observed that agglomeration of many micro-fine particles with a diameter of about 20 nm for NiO@WO_3@bentonite nanocomposite, which leads to a rough surface and the presence of a porous structure. This conclusion was evidenced by the high surface area of the resultant NiO@WO_3@bentonite nanocomposite.

X-ray Diffraction analysis of the Modified Bentonite Adsorbents

The crystalline structure of the adsorbents was confirmed by powder X-Ray Diffraction (XRD) using a Siemens D-500 X-ray diffractometer equipped with Ni-filtrated CuKα radiation (40 kV tube voltage, 100 mA tube current and λ= 0.154 nm) and the chemical composition of bentonite obtained using X-Ray Diffraction (XRD) analysis.

The XRD results indicated the presence of iron oxide (Hematite), silicon oxide (quartz), aluminum silicate hydroxide (Kaolinite), aluminum hydroxide silicate (Montmorillonite), magnesium aluminum silicon oxide hydroxide hydrate (Palygorskite), calcium strontium aluminum silicate hydrate (Chabazite-Ca), silicon oxide (Cristobalite). The 2θ scanning angle range was 5−80° with a step of 0.02 deg/s. X-ray diffraction analysis in Fig.7 was carried out to identify the mineralogical structure of the modified bentonite sorbents. The sharp diffraction peaks of the bentonite were due to the feature of Montmorillonite, which showed characteristic reflections at 2θ = 7.87°. The sharp peak of the Palygorskite showed characteristic reflections at 2θ = 8.57°. The diffraction peaks at 2θ = 9.89° represent Chabazite-Ca. The diffraction

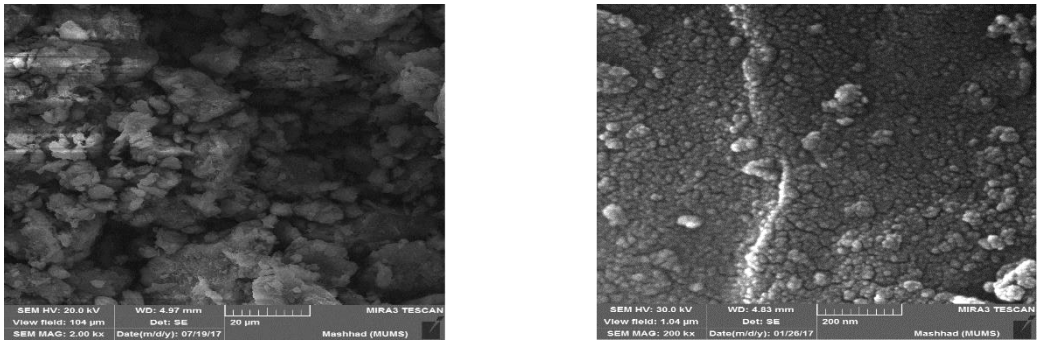

Fig. 6: a) SEM images of raw bentonite. b) SEM images of NiO@WO$_3$@bentonite.

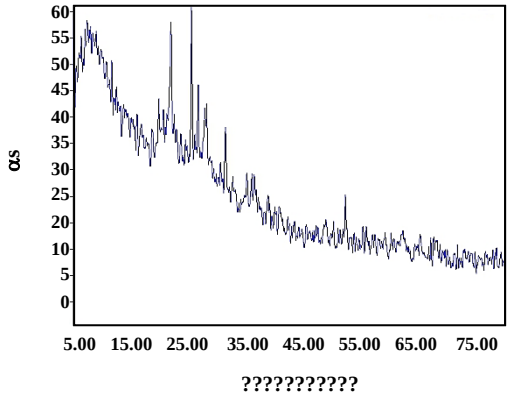

Fig. 7: XRD spectra of NiO@WO$_3$@bentonite.

reflections at 2θ = 21.96° show the presence of Cristobalite. Also, the sharp peak at 2θ = 33.23° shows the presence of Hematite. The diffraction peaks at 2θ = 36.62° and 26.7° represent the Quartz.

Experimental design

Screening of significant factors using PBD

In this paper, modified bentonites were used and evaluated by experimental design. Although a large number of factors influence this process, some of them do not have a significant effect on it. Screening designs are used to determine the main important factors and their interactions with all potential factors [42]. PBD is a valuable practical design to screen the significant variables of a process [43]. So, the screening design was applied mostly. The significant factors of the appraisal model can be identified by analysis of variance (ANOVA) [44]. The Placket–Burman (PB) factorial design can identify major factors affecting DBT adsorption and extraction by a relatively small number of experiments. Table 4 shows the experimental layout for the 12-run PBD with response values (as current peak heights) in two levels of factors. According to the preliminary experiments, sorbent amount, solution volume, temperature, mix rate, time, solvent kind, solvent volume, and time of sonication with two levels were the considered variables for modified bentonite. Table 4 shows the experimental layout for the 12-run PBD with response values (as current peak heights) in two levels of factors. Fig. 8 illustrates the standardized Pareto plot of the main effects for the PBD. The Pareto plot shows that effects of sorbent amount, solution volume, extraction solvent volume and extraction solvent kind are most important to the process, thus these factors should be studied at a greater depth. Based on the preliminary experiments, variations in the parameters considered might affect the analytical signal. It was studied using Central Composite Design (CCD).

Optimization using CCD

The optimization approach frequently starts with a screening design to select the essential factors and it proceeds with an optimization design for example Taguchi design, Central Composite Design (CCD), Doehlert Matrix (DM), or Box–Behnken Design (BBD) [45]. CCD was shown to be well efficient compared with other designs such as BBD and DM [46]. A CCD combines a two-level full or fractional factorial design with extra points (star points) and at least one point at the center of the experimental region this point is selected to obtain various properties, for example, reliability or orthogonality [44]. This design consists of a full factorial design (23 hypercube points, 2×3 axial points, and 6 replicates of center points).

Table 4: The results of PB experimental design matrix.

Standard order	Run order	Blocks	Sorbent amount (g)	volume	T	Rate (rpm)	Time (min)	Solvent	Volume Solvent	Time Sonic (min)	A
1	1	1	0.008	5	60	3000	20	methanol	10	30	0.450
2	2	1	0.008	10	25	5000	20	methanol	5	30	0.701
3	3	1	0.004	10	60	3000	40	methanol	5	10	0.453
4	4	1	0.008	5	60	5000	20	ethanol	5	10	0.440
5	5	1	0.008	10	25	5000	40	methanol	10	10	0.450
6	6	1	0.008	10	60	3000	40	ethanol	5	30	0.590
7	7	1	0.004	10	60	5000	20	ethanol	10	10	0.220
8	8	1	0.004	5	60	5000	40	methanol	10	30	0.170
9	9	1	0.004	5	25	5000	40	ethanol	5	30	0.210
10	10	1	0.008	5	25	3000	40	ethanol	10	10	0.330
11	11	1	0.004	10	25	3000	20	ethanol	10	30	0.218
12	12	1	0.004	5	25	3000	20	methanol	5	10	0.290

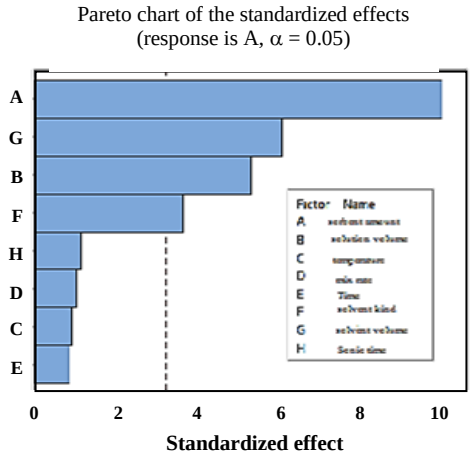

Fig. 8: The standardized main effect Pareto chart for PBD.

In this paper, four factors; two-level CCD with 31 runs was employed. Table 5 shows CCD and current peak heights for modified bentonite. The aim of this analysis is to maximize these responses estimated for the average value of four signals obtained under the same experimental conditions.

The purpose of this analysis is to maximize these responses estimated for the average value of four signals obtained under the same experimental situation by applying regression analysis to experimental data. The results of CCD were fitted with a polynomial equation for each response. The following quadratic models expressed an empirical relationship between response and input variables in un-coded values:

A: 2.947 - 3.82 g -0.1701 solvent volume + 0.03303 volume + 0.001487 %methanol + 2.783 g×g + 0.01333 solvent volume × solvent volume – 0.0659 g × solvent volume – 0.002487 solvent volume × volume – 0.000095 volume × %methanol

R^2 and adjusted R^2 were obtained 99.57% and 99.35% for the modified model, respectively. Table 6 shows the analysis of variance (ANOVA) results for this regression model. The maximum p-value for lack-of-fit i.e. 0.082 (p-value > 0.05) were obtained for modified. According to the method proposed by Derringer and Such [47], the optimal conditions were obtained 0.01 g, 12 cm^3, 60 ˚C, 3000 rpm, 20 min,100% methanol, 3 cm^3, 30 min for sorbent amount, solution volume, temperature, rate, time, %extraction solvent, extraction solvent volume, and sonication time respectively. At the optimal conditions, the predicted responses of conditions and responses to the applied desirability, and desulfurization method were performed.

Table 5: The CCD matrix and the experimental results.

Standard order	Run order	PtType	Blocks	Sorbent amount (g)	Solution volume	Methanol %	Volume Solvent	A
1	1	1	1	0.006	7	50	3	1.350
2	2	1	1	0.01	7	50	3	1.530
3	3	1	1	0.006	7	50	7	0.951
4	4	1	1	0.01	7	50	7	1.044
5	5	1	1	0.006	12	50	3	1.450
6	6	1	1	0.01	12	50	3	1.630
7	7	1	1	0.006	12	50	7	0.960
8	8	1	1	0.01	12	50	7	1.128
9	9	1	1	0.006	7	100	3	1.400
10	10	1	1	0.01	7	100	3	1.590
11	11	1	1	0.006	7	100	7	0.954
12	12	1	1	0.01	7	100	7	1.105
13	13	1	1	0.006	12	100	3	1.455
14	14	1	1	0.01	12	100	3	1.680
15	15	1	1	0.006	12	100	7	0.980
16	16	1	1	0.01	12	100	7	1.132
17	17	-1	1	0.006	9.5	75	5	1.110
18	18	-1	1	0.01	9.5	75	5	1.320
19	19	-1	1	0.009	9.5	75	3	1.480
20	20	-1	1	0.009	9.5	75	7	1.001
21	21	-1	1	0.009	7	75	5	1.135
22	22	-1	1	0.009	12	75	5	1.250
23	23	-1	1	0.009	9.5	50	5	1.190
24	24	-1	1	0.009	9.5	100	5	1.200
25	25	0	1	0.009	9.5	75	5	1.`196
26	26	0	1	0.009	9.5	75	5	1.174
27	27	0	1	0.009	9.5	75	5	1.195
28	28	0	1	0.009	9.5	75	5	1.180
29	29	0	1	0.009	9.5	75	5	1.199
30	30	0	1	0.009	9.5	75	5	1.178
31	31	0	1	0.009	9.5	75	5	1.195

Table 6: The ANOVA results for evaluation of mathematical models of sensitivity in relation to electrode preparation factors, obtained by response surface design.

Source	DF[a]	Adj SS[b]	Adj MS[d]	F -Value	p-Value
ANOVA for five exprimental					
Linear	4	1.18955	0.29739	1086.41	0.000
Square	2	0.04377	0.02189	79.96	0.000
Residual error	21	0.00575	0.00027		
Lack-of-fit	15	0.00511	0.00034	3.18	0.081
Pure error	6	0.00064	0.00011		
Total	30	1.24489			

a) Degrees of freedom, b) Adjusted sum of squares, c) Adjusted mean squares

In the optimal condition, the predicted desulfurization rate was equal to 99.4 %, and the amount of the remaining DBT was equal to 0/59 ppm.

Interpretation of residual graphs

One technique of testing for a normal distribution is to determine how closely the points on a normal probability plot conform to a direct line. Minitab normally gives the usual probability plot directly as depicted in Fig. 9. The usual probability plot is a helpful instrument for indicating the normal distribution of residuals. In this plot, the points pursue a straight line. It is evident from this test that the data were normally distributed. The study of residuals (the difference between the experimental and the predicted value) is an essential component in interpreting models. For an excellent model, the residuals should be randomLy and normally distributed. In Fig. 9 the plot of residuals against the fitted values is provided and the residuals do not explain any particular sample and are approximately usually distributed. The histogram in Fig. 9 shows a distribution of measurements around symmetrical the mean with most of the measurements clustered around the center of the graph suggestive of a normal distribution of the residuals without any outlier. The final graph of residual against observation order is balanced and centered close to zero with no clear outlier in the observation order.

Effect of calcination temperature on the performance of adsorption desulfurization

Different calcination temperatures range from (110 °C) to (500 °C) were tested on bentonite loaded with W and Ni. Under the different calcination temperatures, the static desulfurization effects of the absorbents were collected. The calcination temperature has a strong influence on the desulfurization performance of the modified bentonite sorbents. It revealed that the best calcination temperature of the modified bentonite adsorbents was 400 °C. As the calcination temperature increased from 110 °C to 500 °C, the breakthrough time and sulfur removal ability of the adsorbents were gradually increased.

CONCLUSIONS

In this research, a novel adsorbent has been successfully synthesized and its adsorption behavior was examined. The nanocomposite NiO@WO_3@bentonite was investigated for adsorptive desulfurization (ADS) as a nano sorbent. W and Ni have been found effective for the removal of sulfur compounds from commercial diesel. Experimental adsorption results show that NiO@WO_3@bentonite exhibits high adsorption capacity for DBT solution with maximum adsorption capacities of 93.5 % which is a large amount higher than another similar adsorbent. The direct interaction between the sulfur compounds in diesel and the surface of the NiO and WO_3 plays the main role, indicating that NiO and WO_3 adsorbents are well for desulfurization. The Langmuir isotherms best represent the equilibrium adsorption data. Thus, considering the simple synthesis procedure, low cost, high removal efficiency, excellent stability, and easy separation, NiO@WO3@ bentonite appears to have good potential for use in removing radioactive DBT in liquid fuel.

Acknowledgment

The authors appreciate Payame Noor University's support of the research.

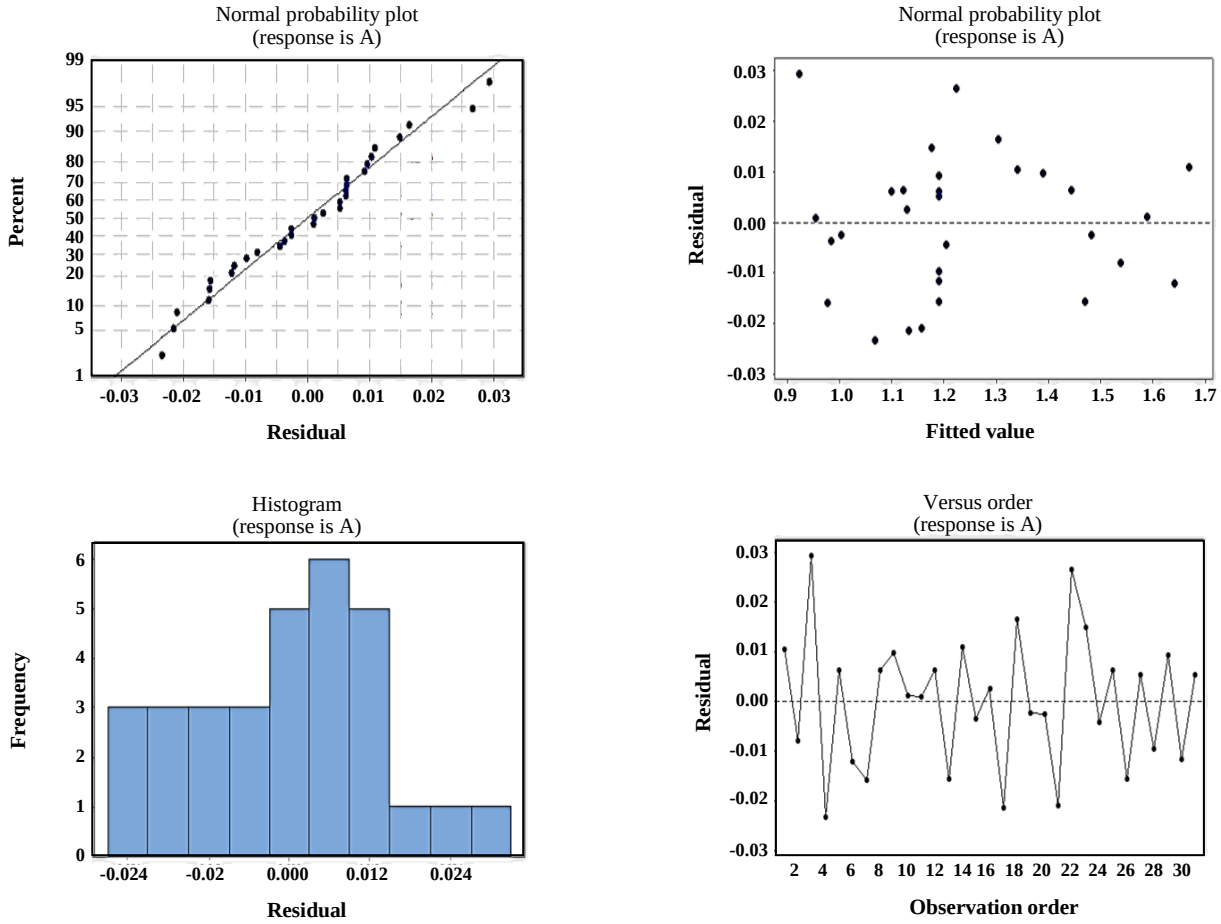

Fig. 9: Residual Plots for % Removal of DBT.

Received : Oct.. 29, 2020 ; Accepted : Jan. 18, 2021

REFERENCES

[1] Kaufmann T.G., Kaldor A., Stuntz G.F., Kerby M.C., Ansell L.L., Catalysis Science and Technology for Cleaner Transportation Fuels, *Catal. Today*, **62(1)**: 77-90 (2000).

[2] Song C., An Overview of New Approaches to Deep Desulfurization for Ultra-Clean Gasoline, Diesel Fuel and Jet Fuel, *Catal. Today*, **86(1)**: 211-263 (2003).

[3] Nakhaei A., Ramezani S., Synthesis, Characterization, and Theoretical Studies of the New Antibacterial Zn (II) Complexes from New Fluorescent Schiff Bases Prepared By Imidazo [4', 5': 3, 4] benzo [1, 2-c] Isoxazole, *Iran. J. Chem. Chem. Eng. (IJCCE)*, **38(4)**: 79-90 (2019).

[4] Jiang M., Ng F.T.T., Rahman A., Patel V., Flow Calorimetric and Thermal Gravimetric Study of Adsorption of Thiophenic Sulfur Compounds on NaY Zeolite, *Thermochim. Acta*, **434(1)**: 27-36 (2005).

[5] Jiang M., Ng F.T.T., Adsorption of Benzothiophene on Y Zeolites Investigated by Infrared Spectroscopy and Flow Calorimetry, *Catal. Today*, **116(4)**: 530-536 (2006).

[6] Yadegarian S., Davoodnia A., Nakhaei A., Solvent-Free Synthesis of 1, 2, 4, 5-tetrasubstituted Imidazoles Using Nano Fe_3O_4@ SiO_2-OSO_3H as a Stable and Magnetically Recyclable Heterogeneous Catalyst, *Orient. J. Chem.*, **31(1)**: 573-579 (2015).

[7] Mikhail S., Zaki T., Khalil L., Desulfurization by an Economically Adsorption Technique, *Appl. Catal. A-Gen.*, **227(1)**: 265-278 (2002).

[8] Park J.G., Ko C.H., Yi K.B., Park J.-H., Han S.-S., Cho S.-H., Kim J.-N., Reactive Adsorption of Sulfur Compounds in Diesel on Nickel Supported on Mesoporous Silica, *Appl. Catal. B*, **81(3)**: 244-250 (2008).

[9] Hernández-Maldonado A.J., Yang F.H., Qi G., Yang R.T., Desulfurization of Transportation Fuels by Π-Complexation Sorbents: Cu(I)-, Ni(II)-, and Zn(II)-zeolites, *Appl. Catal. B*, **56(1)**: 111-126 (2005).

[10] Nakhaei A., Davoodnia A., Yadegarian S., Nano-Fe3O4@ ZrO2-SO3H as Highly Efficient Recyclable Catalyst for the Green Synthesis of Fluoroquinolones in Ordinary or Magnetized Water, *Iran. J. Catal.*, **8(1)**: 47-52 (2018).

[11] Ma X., Velu S., Kim J.H., Song C., Deep Desulfurization of Gasoline by Selective Adsorption over Solid Adsorbents and Impact of Analytical Methods on Ppm-Level Sulfur Quantification for Fuel Cell Applications, *Appl. Catal. B*, **56(1)**: 137-147 (2005).

[12] Pan D.-q., Fan Q.-h., Li P., Liu S.-p., Wu W.-s., Sorption of Th(IV) on Na-bentonite: Effects of pH, Ionic Strength, Humic Substances and Temperature, *Chem. Eng.*, **172(2)**: 898-905 (2011).

[13] Wang S., Dong Y., He M., Chen L., Yu X., Characterization of GMZ Bentonite and Its Application in the Adsorption of Pb(II) from Aqueous Solutions, *Appl. Clay Sci.*, **43(2)**: 164-171 (2009).

[14] Davoodnia A., Nakhaei A., Basafa S., Tavakoli-Hoseini N., Investigating Effect of Cerium (IV) Sulfate Tetrahydrate as Reusable and Heterogeneous Catalyst for the One-Pot Multicomponent Synthesis of Polyhydroquinolines, *Adv. J. Chem. A*, **1**(2. pp. 66-126): 96-104 (2018).

[15] Fan H., Shangguan J., Liang L., Shen F., Li C., Reduction Behavior of Iron Oxide Sorbent and Its Effect on Sulfidation, *Energy Fuels*, **24(7)**: 3784-3788 (2010).

[16] Renedo M.J., González F., Pesquera C., Fernández J., Study of Sorbents Prepared from Clays and CaO or $Ca(OH)_2$ for SO_2 Removal at Low Temperature, *Ind. Eng. Chem. Res.*, **45(10)**: 3752-3757 (2006).

[17] Ersoy-Mericboyu A., Removal of Sulphur Dioxide from Flue Gases, *Energy Sources*, **21(7)**: 611-619 (1999).

[18] Nakhaei A., Shojaee S., Yaghoobi E., Ramezani S., Fast and Green Synthesis of 3, 4-dihydropyrimidin-2 (1h)-Ones And-Thiones Using Nanometasilica Disulfuric Acid as Recyclable Catalyst in Water, *Heterocycl. Lett.*, **7(2)**: 323-331 (2017).

[19] Froehner S., Machado K.S., Falcão F., Adsorption of Dibenzothiophene by Vermiculite in Hydrophobic Form, Impregnated with Copper Ions and in Natural Form, *Water Air Soil Pollut.*, **209(1-4)**: 357-363 (2010).

[20] Wu T., Yan X., Cai X., Tan S., Li H., Liu J., Yang W., Removal of Chattonella Marina with Clay Minerals Modified with a Gemini Surfactant, *Appl. Clay Sci.*, **50(4)**: 604-607 (2010).

[21] Gu L., Xu J., Lv L., Liu B., Zhang H., Yu X., Luo Z., Dissolved Organic Nitrogen (DON) Adsorption by Using Al-Pillared Bentonite, *Desalination*, **269(1)**: 206-213 (2011).

[22] Feng J., Hu X., Yue P.L., Novel Bentonite Clay-Based Fe−Nanocomposite as a Heterogeneous Catalyst for Photo-Fenton Discoloration and Mineralization of Orange II, *Environ. Sci. Technol.*, **38(1)**: 269-275 (2004).

[23] Rezala H., Khalaf H., Valverde J.L., Romero A., Molinari A., Maldotti A., Photocatalysis with Ti-Pillared Clays for the Oxofunctionalization of Alkylaromatics by O_2, *Appl. Catal. A-Gen.* , **352(1)**: 234-242 (2009).

[24] Wang J., Xu F., Xie W.-j., Mei Z.-j., Zhang Q.-z., Cai J., Cai W.-m., The Enhanced Adsorption of Dibenzothiophene onto Cerium/Nickel-Exchanged Zeolite Y, *J. Hazard. Mater.*, **163(2)**: 538-543 (2009).

[25] Griffith C.S., Luca V., Ion-Exchange Properties of Microporous Tungstates, *Chem. Mater.*, **16(24)**: 4992-4999 (2004).

[26] Griffith C.S., Luca V., Hanna J.V., Pike K.J., Smith M.E., Thorogood G.S., Microcrystalline Hexagonal Tungsten Bronze. 1. Basis of Ion Exchange Selectivity for Cesium and Strontium, *Inorg. Chem.*, **48**(13): 5648-5662 (2009).

[27] Darvishi Z., Morsali A., Synthesis and Characterization of Nano-Bentonite by Sonochemical Method, *Ultrason. Sonochem.*, **18(1)**: 238-242 (2011).

[28] Holford I.C.R., Wedderburn R.W.M., Mattingly G.E.G., A Langmuir Two-Surface Equation as a Model for Phosphate Adsorption by Soils, *J. Soil Sci.*, **25(2)**: 242-255 (1974).

[29] Nakhaei A., Yadegarian S., An Efficient Synthesis of 14-substituted-14H-dibenzo [a, j] Xanthene Derivatives Promoted by a Nano Isopolyoxomolybdate under Thermal and Solvent-Free Conditions, *Iran. J. Org. Chem.*, **9(2)**: 2057-2065 (2017).

[30] Abdulkarim M., Al-Rub F.A., Adsorption of Lead Ions from Aqueous Solution onto Activated Carbon and Chemically-Modified Activated Carbon Prepared from Date Pits, *Adsorp. Sci. Technol.*, **22(2)**: 119-134 (2004).

[31] Wu F.-C., Tseng R.-L., Juang R.-S., Role of pH in Metal Adsorption from Aqueous Solutions Containing Chelating Agents on Chitosan, *Ind. Eng. Chem. Res.*, **38(1)**: 270-275 (1999).

[32] Inbaraj B.S., Sulochana N., Mercury Adsorption on a Carbon Sorbent Derived from Fruit Shell of Terminalia Catappa, *J. Hazard. Mater.*, **133(1)**: 283-290 (2006).

[33] Eren E., Afsin B., Investigation of a Basic Dye Adsorption from Aqueous Solution onto Raw and Pre-Treated Bentonite Surfaces, *Dyes Pigm.*, **76(1)**: 220-225 (2008).

[34] Liu X.-H., Luo X.-H., Lu S.-X., Zhang J.-C., Cao W.-L., A Novel Cetyltrimethyl Ammonium Silver Bromide Complex and Silver Bromide Nanoparticles Obtained by the Surfactant Counterion, *J. Colloid Interface Sci.*, **307(1)**: 94-100 (2007).

[35] Ayodele O.B., Lim J.K., Hameed B.H., Pillared Montmorillonite Supported Ferric Oxalate as Heterogeneous Photo-Fenton Catalyst for Degradation of Amoxicillin, *Appl. Catal. A-Gen.*, **413-414**: 301-309 (2012).

[36] Tireli A.A., Marcos F.C.F., Oliveira L.F., Guimarães I.d.R., Guerreiro M.C., Silva J.P., Influence of Magnetic Field on the Adsorption of Organic Compound by Clays Modified with Iron, *Appl. Clay Sci.*, **97-98**: 1-7 (2014).

[37] Nakhaei A., Davoodnia A., Yadegarian S., An Efficient Green Approach for the Synthesis of Fluoroquinolones Using Nano Zirconia Sulfuric Acid as Highly Efficient Recyclable Catalyst in Two Forms of Water, *Iran. J. Chem. Chem. Eng. (IJCCE)*, **37(3)**: 33-42 (2018).

[38] Manjanna J., Kozaki T., Sato S., Fe(III)-Montmorillonite: Basic Properties and Diffusion of Tracers Relevant to Alteration of Bentonite in Deep Geological Disposal, *Appl. Clay Sci.*, **43(2)**: 208-217 (2009).

[39] Tyagi B., Chudasama C.D., Jasra R.V., Determination of Structural Modification in Acid Activated Montmorillonite Clay by FT-IR Spectroscopy, *Spectrochim. Acta A*, **64(2)**: 273-278 (2006).

[40] Kanthimathi M., Dhathathreyan A., Nair B.U., Nanosized Nickel Oxide using Bovine Serum Albumin as Template, *Mater. Lett.*, **58(22)**: 2914-2917 (2004).

[41] Nakhaei A., Ramezani S., Shams-Najafi S.J., Farsinejad S., Nano-Fe_3O_4@ ZrO_2-SO_3H as Highly Efficient Recyclable Catalyst for the Green Synthesis of Fluoroquinolones, *Lett. Org. Chem.*, **15(9)**: 739-746 (2018).

[42] Nezhadali A., Mojarrab M., Computational Study and Multivariate Optimization of Hydrochlorothiazide Analysis using Molecularly Imprinted Polymer Electrochemical Sensor Based on Carbon Nanotube/Polypyrrole Film, *Sens. Actuat. B Chem.*, **190**: 829-837 (2014).

[43] Kennedy M., Krouse D., Strategies for Improving Fermentation Medium Performance: A Review, *J. Ind. Microbiol. Biotechnol.*, **23(6)**: 456-475 (1999).

[44] Plackett R.L., Burman J.P., The Design of Optimum Multifactorial Experiments, *Biometrika*, **33(4)**: 305-325 (1946).

[45] Sharif K.M., Rahman M.M., Azmir J., Mohamed A., Jahurul M.H.A., Sahena F., Zaidul I.S.M., Experimental Design of Supercritical Fluid Extraction – A Review, *J. Food Eng.*, **124**: 105-116 (2014).

[46] Zolgharnein J., Shahmoradi A., Ghasemi J.B., Comparative Study of Box–Behnken, Central Composite, and Doehlert Matrix for Multivariate Optimization of Pb (II) Adsorption onto Robinia Tree Leaves, *J. Chemom.*, **27(1-2)**: 12-20 (2013).

[47] Tarley C.R.T., Silveira G., dos Santos W.N.L., Matos G.D., da Silva E.G.P., Bezerra M.A., Miró M., Ferreira S.L.C., Chemometric Tools in Electroanalytical Chemistry: Methods for Optimization Based on Factorial Design and Response Surface Methodology, *Microchem. J.*, **92(1)**: 58-67 (2009).